

## Research Article

Hongwei Sun, Xiaopeng Lin, Xiaoyan Gu\*, Chenfu Fang, and Zhidong Yang

# Effect of post-weld heat treatment on the microstructure and mechanical properties of laser-welded joints of SLM-316 L/rolled-316 L

<https://doi.org/10.1515/htmp-2022-0235>

received April 24, 2022; accepted August 08, 2022

**Abstract:** Connecting small pieces of parts manufactured by Selective Laser Melting (SLM) and traditional formed parts into large structural component by using welding technology provides a high-efficiency and low-cost way for expanding additive manufacturing technology. SLMed parts usually exhibit similar or superior tensile strength but lower ductility compared to that of cast or rolled ones due to the rapid cooling and cyclic heating deposition characteristics. What about the weldability of the dissimilar joints of SLMed parts and rolled ones? Whether the properties of the welded joints can be improved by heat treatment under the premise of ensuring the reliability of the joint is unclear. The weldability and the effect of heat treatment temperature on the microstructure and properties of laser-welded joints of SLM-316 L/rolled-316 L are studied in this article. The results show that the joints exhibit good weldability without obvious defects. The low temperature annealing treatment had no significant effect on the multi-layered structure and columnar austenite grains, but only changed the morphology and content of ferrite within the grains leading to the slight increase of elongation but decrease of material strength. The corrosion performance was almost unaffected. After solution annealing above 1,000°C, the ferrite was nearly dissolved in the austenite matrix. The austenite recrystallized and the multilayered structure was destroyed, which resulted in decrease of material strength, a slightly improvement in corrosion resistance,

and the elongation was greatly enhanced. After the detailed study, it was concluded that the post-weld heat treatment provided an effective way for improving the overall performance of the SLM-316 L/rolled-316 L dissimilar joint.

**Keywords:** post-weld heat treatment, mechanical properties, selective laser melting, laser-welded, corrosion

## 1 Introduction

Selective laser melting (SLM), as one of the most representative additive manufacturing technology, has great advantages in rapid and free manufacturing of 3D structure with the characteristics of good surface roughness and high geometric precision [1,2]. However, the restriction on the availability of large-scale SLM equipment, the control of defects and dimensional accuracy, and the residual stress associated with SLM complex thermal process limit the application of SLM on large-scale components [3,4]. Connecting small pieces of parts manufactured by SLM and traditional formed parts into large structural component by using welding technology provides available way for expanding additive manufacturing technology. On the one hand, high-efficiency, low-cost production is achieved. On the other hand, the residual stress in the manufacturing of large-scale parts can be relieved, and the quality and forming accuracy of the welded structure are controlled more easily.

However, dissimilar welded joints encountered many associated structural integrity problems such as differences in thermal expansion coefficient, carbon migration, mismatched mechanical property, and other discontinuities like environmentally assisted problems, formation of carbon-rich, and depleted zones [5–7]. Post-weld heat treatment (PWHT) is usually an effective measure to solve the above problems. Sirohi et al. [8] had investigated heat treatment on the mechanical performance of the GTA welded dissimilar joint of P91 and SS304H steel. After PWHT, an increase in the density of Mo and Nb-enriched

\* **Corresponding author: Xiaoyan Gu**, School of Materials and Technology, Jiangsu Key Laboratory of Advanced Welding Technology, Jiangsu University of Science and Technology, Zhenjiang 212003, China, e-mail: liligu1983@163.com

**Hongwei Sun:** Department of Technology, Jiangsu Automation Research Institute, Lianyungang 222006, China

**Xiaopeng Lin, Chenfu Fang, Zhidong Yang:** School of Materials and Technology, Jiangsu Key Laboratory of Advanced Welding Technology, Jiangsu University of Science and Technology, Zhenjiang 212003, China

particles were observed, and a soft pro-eutectoid ferrite and hard zone were formed near the interface due to the C and Cr diffusion. An increase in both tensile strength and % elongation was measured after the PWHT. Sirohi et al. [9] conducted systematic study on metallographic characterization and mechanical testing on dissimilar joint of the P91/SS304H steel using the Ni-based super alloy IN617 filler for as-welded (AW) and PWHT conditions. The PWHT showed a drastic reduction in residual stress value in a different zones of the weldments and lower impact energy of the weld metal.

PWHT is also adopted to solve some problems occurring in SLM process, such as sub-crystalline structure with high-density dislocation, epitaxial columnar crystals, accumulation of residual stress, and poor ductility of components due to the characteristic of layer-by-layer forming and non-equilibrium solidification of base materials during the SLM. In order to meet the requirements of the microstructure and mechanical properties of the formed parts, the corresponding post-heat treatment of SLM formed parts were carried out. Karabulut et al. [10] conducted several heat treatments on SLMed superalloy In718, and found that appropriate post-heat treatment can increase the toughness of the morphologic alloy. Yan et al. [11] used SLM technology instead of welding to connect  $\text{Ti}_6\text{Al}_4\text{V}$  and conducted post-heat treatment. The results showed that the post-heat treatment process significantly changed the mechanical properties of formed parts, because the post-heat treatment changed the width, length, and distribution of Pt phase that would affect the properties. Liu et al. [12] compared the microstructure evolution, hardness, and wear resistance properties of  $\text{NiCrSiB} + x\text{Y}_2\text{O}_3$  formed by SLM under three different heat treatment conditions (solid solution, solid solution aging, and annealing). It is found that carbide and brittle phase appear in solution and solution aging stage, and the grain is refined after annealing treatment, and the properties are further improved. Åsberg et al. [13] evaluated the microstructure and properties of the hot die steel H13 formed by SLM after direct tempering and quenching and tempering treatment, respectively. The results showed that the cell/dendrite morphology and local hardness uneven phenomenon caused by SLM forming were eliminated by post-heat treatment, and the hardness of the tempered sample was high enough without affecting the fracture toughness. Shin et al. [14] found that the microstructure stability and mechanical properties of SLM formed 316 LSS stainless steel changed after annealing at a certain temperature. When the annealing temperature reached 400°C, the yield strength increased by 10% and elongation

decreased not significantly because of the thermal stability of the crystal cell/dislocation structure. However, when the annealing temperature is higher than 400°C, the microstructure thermal stability is destroyed and silicate dissolves, which leads to the strength reduction. The above provides a possibility for controlling the properties of laser additive manufacturing forming parts.

One the most significant issues to be considered for the austenitic stainless steel joints is to avoid chromium carbide formation in the grain and grain boundaries of the weld zone. The PWHT might be an advantage for eliminating carbide precipitates and improving the tensile strength of joints since it could regiment the microstructure especially at the weld zone [15]. Ghorbani et al. [16] investigated the effects of PWHT on the microstructure, mechanical properties, and corrosion properties of the welded joint. Heat treatment of the whole series of samples at 860°C and 960°C can eliminate chromides generated during welding and homogenize the microstructure. Jiang et al. [17] studied the microstructural, tensile strength, and hardness of tungsten inert gas-welded CLAM steel joints, subjected to PWHT at 740°C for 1 h. They conducted the mechanical and micro structural tests on the welded joints and the result showed that the mechanical properties of the CLAM steel welded joints can be improved by a reasonable PWHT. Li et al. [18] investigated the different PWHT to achieve a good combination of strength, toughness, and corrosion properties.

Welding method is also one of the key factors affecting the quality of dissimilar metal joints. The existing welding techniques like gas metal arc welding need the preheating, inter-pass heating that causes the distortion and localized softening of the weld metal [19]. To overcome such difficulties, radiant beam-welding processes like laser beam welding and electron beam welding have been suggested, which improves the welds' quality and produces the weld joint with lesser distortion and narrow heat affected zone (HAZ) [20].

In this study, 316 L stainless steel rolled plates with 3 mm thickness were connected with SLMed ones by laser welding and the acquired butt joints were then subjected to low temperature annealing (LTA) at 400°C for 4 h and solution treatment (ST) at 1,050°C for 30 min. The study focused on the effect of varying heat treatments on homogeneity across the welded joint in terms of microstructural evolution, mechanical properties, and corrosion resistance of welded joints, which provides a theoretical basis for the performance improvement of components prepared by additive manufacturing.

**Table 1:** Chemical compositions of 316 L stainless steel powders (wt%)

C	Si	Mn	P	S	Ni	Cr	Mo
0–0.03	0–1.0	0–2.00	0–0.045	0–0.03	10–14	16–18	2–3

## 2 Experimentation

The SLM experiments were conducted on the industrial-grade 3D printer EOS M290, which includes a continuous wave ytterbium-doped fiber laser (maximum output power of 400 W), an automatic powder feeding device, a 3D building platform, and a set of control system. The original material for SLM in this experiment was 316 L stainless steel powder, which was purchased from Jiangsu VILORY New Material Technology Co., Ltd, with the size in the range of 20–50  $\mu\text{m}$  prepared by the vacuum induction smelting gas-atomized method. The chemical composition is shown in Table 1.

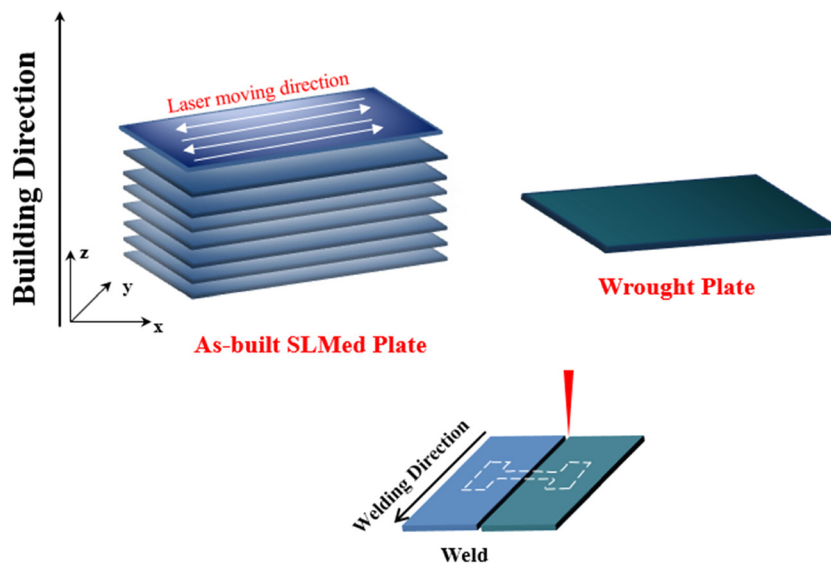
The gas-atomized spherical 316 L powders were then deposited layer-by-layer on a 316 L stainless steel substrate through the 3D printer in an argon environment with oxygen concentration controlled below 50 ppm. Cuboid samples with dimension of 65 mm  $\times$  30 mm  $\times$  25 mm were constructed for follow-on use. The as-built samples were cut from the substrate and annealed at 650°C for 2 h in a box furnace (KSX-8-1100G) to release the residual stress, and then sliced into thin plates with a dimension of 65 mm  $\times$  30 mm  $\times$  3 mm by wire-electrode cutting to be welded. The sliced plates were brushed to remove the oxide film on the surface by sanding treatment.

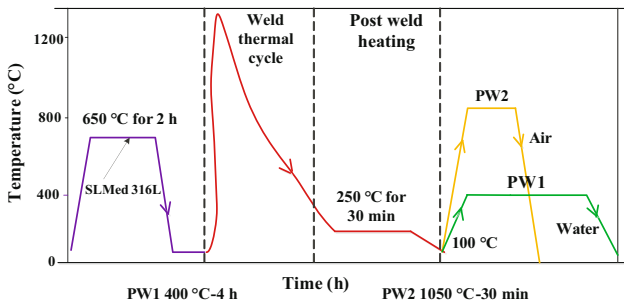
A 6 kW fiber laser (IPG YLS.6000.S2T) with a wave length of 1,070 nm was employed to join the SLM-316 L plates and rolled-316 L ones. During the welding process, the laser beam transmitted through a core fiber with a diameter of 200  $\mu\text{m}$  and focused by a lens with a diameter of 310 mm to get a focused radius of 0.35 mm. The welding supporting facility was ABB six-axis robot, and the laser worked in a multi-mode and continuous output. The laser head was inclined 5° to vertical direction to avoid damage caused by the reflection of the laser beam. In this experiment, the shielding gas used was 99.99% argon flowing out of a paraxial copper gas nozzle. The applied welding parameters are shown in Table 2. Schematic diagram of welding between SLMed parts and rolled parts is shown in Figure 1.

The acquired joints were then subjected to LTA at 400°C for 4 h with subsequent water cooling and solution annealing at 1,050°C for 30 min with subsequent air cooling, respectively. The schematic used in Figure 2

**Table 2:** Parameters of laser welding

Laser power ( $P$ )	Welding speed ( $v$ )	Laser defocused distance ( $D$ )	Gas flow rate ( $Q$ )
2.8 kW	30 mm·min <sup>-1</sup>	0 mm	20 L·min <sup>-1</sup>

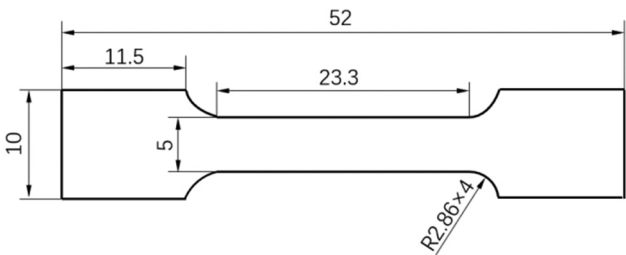
**Figure 1:** Schematic diagram of laser-welded joints' preparation and the tensile samples.



**Figure 2:** Schematic showing the heat treatment performed on base metal and SLM-316 L/rolled-316 L joints.

shows the heat treatment processed on laser-welded joints of SLM-316 L/rolled-316 L.

Metallographic specimens were grinded and polished, and then etched by aqua regia for 10 s to observe the metallography. The macroscopic morphology and microscopic structure were characterized by optical microscope (HAL1000) and scanning electron microscopes (JSM-6480). The Veronese MH5 microhardness tester tested the microhardness of the joints in various locations. Due to the limited size of the sample made by SLM in this experiment, non-standard tensile samples were prepared by proportionally minifying standard ones according to PRC National Standard GB/T228.1-2010. The specific dimension of the welded joints was designed as illustrated in Figure 3. The loading direction of tensile test as well as the laser traveling direction is marked in Figure 1. Phase identification was performed on the laser-welded joints by XRD-6000 using a CuK $\alpha$  radiation with a step size of 0.02° and a dwell time of 1 s per step. The electrochemical tests of all the samples were conducted on a CorrTest EG&G PARC M283 electrochemical station in a three-electrode cell at ambient temperature. The platinum sheet and saturated calomel electrode



**Figure 3:** Tensile sample.

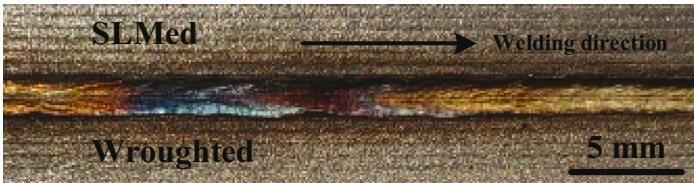

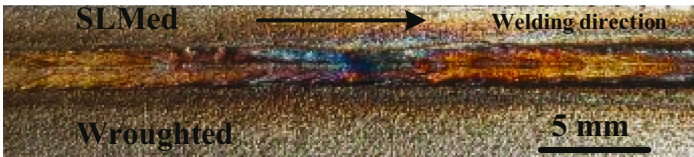
were selected as auxiliary and reference electrodes, respectively. The samples with a size of 10 mm  $\times$  10 mm  $\times$  3 mm were kept in the 3.5 wt% NaCl solution for enough time to obtain potentiodynamic polarization curve. The potential range relative to OCP was from  $-0.5$  to  $1.5$  V at a scanning rate of  $0.5 \text{ mV}\cdot\text{s}^{-1}$ .

### 3 Results and discussion

#### 3.1 Effect of heat treatment on microstructure of welded joint

Table 3 lists the surface morphologies of laser-welded seam in front and back views and the cross-section of joints. As depicted in the images, both the surface and backside of the welds were smooth and uniform, and the microstructure of the weld consists of a large amount of coarse columnar dendrites. The cross-section morphologies of the welded joints exhibited the typical features of laser deep-penetration welding. Obvious convex was observed on the surface of the weld, which was mainly due to the reduction of density and increase of volume

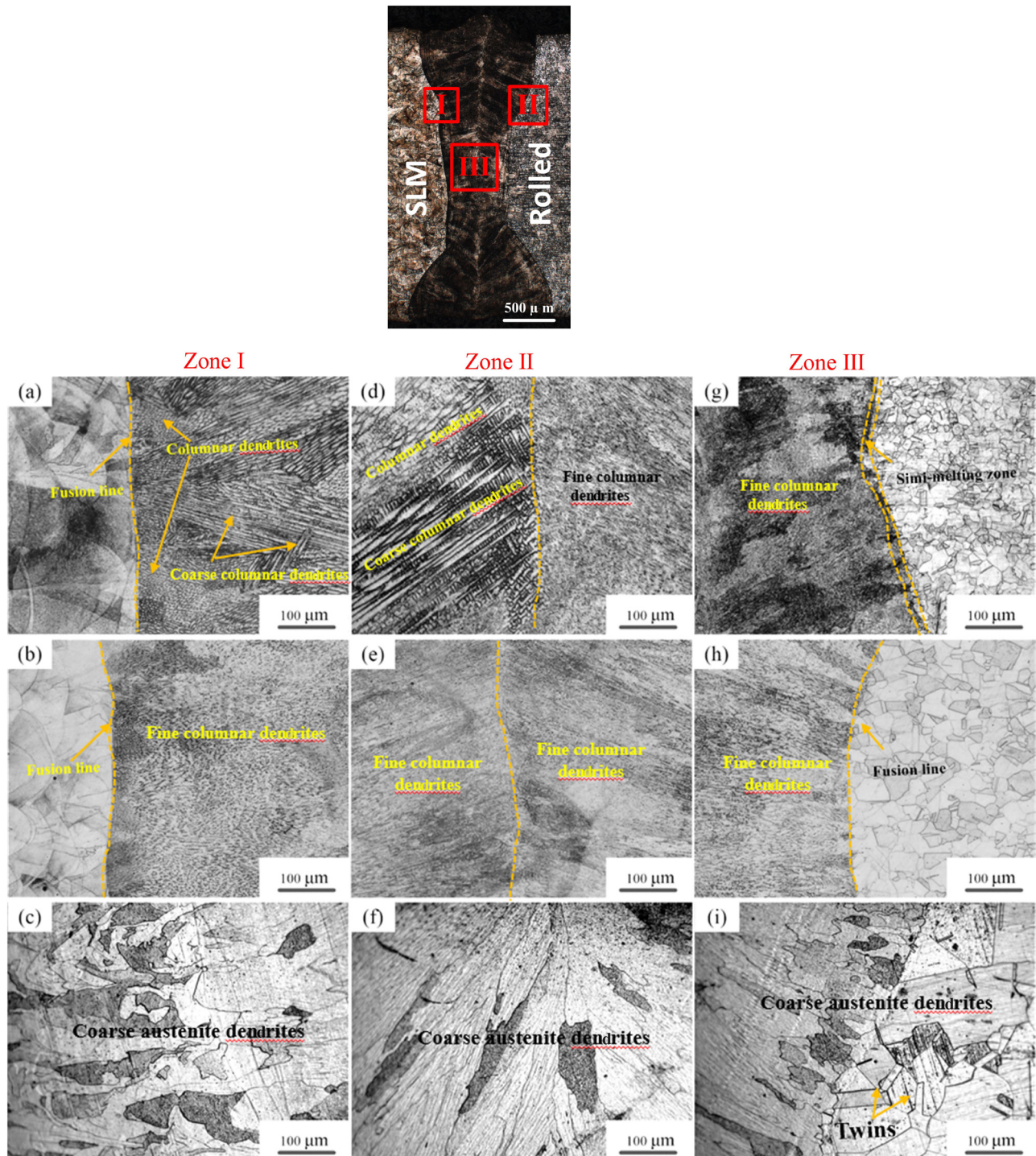
**Table 3:** Surface morphologies of laser-welded seam in front and back views and the cross-section of joints

	Surface morphologies	Cross-section
Weld	<div>Front</div> <div></div>	
	<div>Back</div> <div></div>	



after the rolled/SLMed base metal underwent melting, cooling, and solidification to form weld without external pressure. In addition, the up-thrust of molten material due to the Marangoni flow was also an important factor of the convex [21,22]. The base metal, weld zone, and

fusion zone were discriminated clearly without an apparent transition zone, but the HAZ was not obvious in the welded joints. The fusion line on the SLMed side of the weld was clearer than that on the rolled side. There were no conspicuous defects such as cracks, pores, and non-fusions



**Figure 4:** Microstructure of different areas of weld before and after heat treatment: (a–c) are the microstructure of Zone I, (d–f) are the microstructure of Zone II, (g–i) are microstructure of Zone III of AW joint, the microstructure after annealing treatment at 400°C for 4 h, and ST at 1,050°C for 30 min.

observed in the welded joint, demonstrating that it is feasible to join SLMed parts with rolled ones to obtain reliable welds.

The macroscopic cross-section morphology of joint and the microstructure of each area before and after heat treatment are shown in Figure 4. Figure 4(a–c) are the original microscopic morphology of AW joint, the microstructure after annealing, and ST of Zone I, respectively. Figure 4(d–f) are the original microscopic morphology of AW joint, the microstructure after annealing, and ST of Zone II, respectively. Figure 4(g–i) are the original microscopic morphology of AW joint, the microstructure after annealing, and ST of Zone III, respectively. The microstructure of the SLMed parts is the end-result of metal powder melting and solidification, with adjacent neighboring tracks responsible for partial remelting of the solidified tracks. The morphology displayed compact structures without large holes or cracks, presenting a strong metallurgical bonding formed between melt-tracks. The overlap between adjacent melted tracks and layers was clearly observed from traces of the fusion line region. Periodic regular “fish scales” molten pools were distributed in the SLMed 316 L stainless steel, each of which had roughly the same size and morphology.

A clear fusion line between the weld and the SLMed base metal in Zone I was observed. The microstructure was composed of a layer of columnar dendrites densely arranged at the edge of the weld, which grew perpendicular to the fusion line along the direction of heat dissipation, and a small part of fine cellular crystals. This structure had been extended to the center of the weld.

On the rolled side (Zone II), there was a narrow less conspicuous semi-melting zone between the weld and the base metal instead of the fusion line. The microstructure was mainly dominated by extremely fine columnar crystals perpendicular to the semi-melting zone. Zone III was the center area of the weld. In Zone III, the microstructure on SLMed side was mixed with columnar dendrites and equiaxial crystals of different forms directed toward the center line. The weld on the forged side showed the characteristics of columnar dendrites on the whole, and the grain was much finer than that on the SLMed side. This made the weld appear to be divided into two almost symmetrical parts, which had great differences in microstructure. It is because the microstructure of SLMed parts was mainly in the form of dendrite or columnar crystal, which provided a good nucleation environment for grains. The undercooling degree of the dendrite tip increased with the growth rate. Therefore, in the direction approximately parallel to the interface, the growth rate and the undercooling degree was kept

minimum. In this way, the growth of grains along the dendrite tip, that is, those perpendicular to the interface, exceeded that of dendrites with other orientations [23]. Therefore, the grains on the SLMed side of the weld were more favorable to generate and grow into coarse dendrites than that on the rolled side. Nucleation difficulty on the rolled side resulted in retention of heat in the molten pool, so the grains at the boundary of the base metal appeared semi-melted.

By comparison, it can be seen that the microstructure of the base metal part in the welded joint hardly changed, both the fusion line and the boundary of each micro-molten pool in the SLM forming plane were still clearly observed. Slight refinement of grains in the weld appeared after LTA. ST had a great influence on the microstructure of welded joint. Due to the growth of grains during ST, the original boundary of the micro-molten pool was destroyed and the sub-crystal structure interior were replaced by large grains with irregular shape. Some of the fine grains near the junction between the weld and the base metal crossed through the fusion line to combine into large grains during the growing process. It is worth noting that in the process of merging and growing, the grains in the weld still preferentially grew in the direction of the original grains, that is, perpendicular to the fusion line of the weld towards the center of the weld.

Figure 5 shows the X-ray diffraction (XRD) patterns of the AW joints and heat-treated samples. The crystal indices of AW joints corresponding to the peak were (111), (200), (220), and (311), exhibiting  $\gamma$  austenite (FCC) structure. After the heat treatment at 400°C for 2 h, the XRD patterns have no obvious change, indicating that

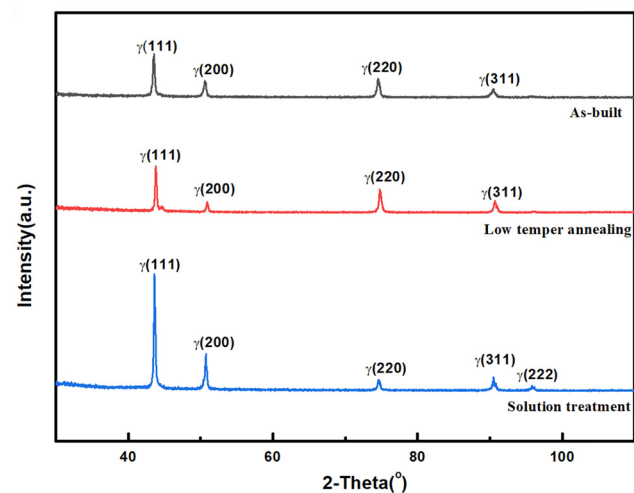
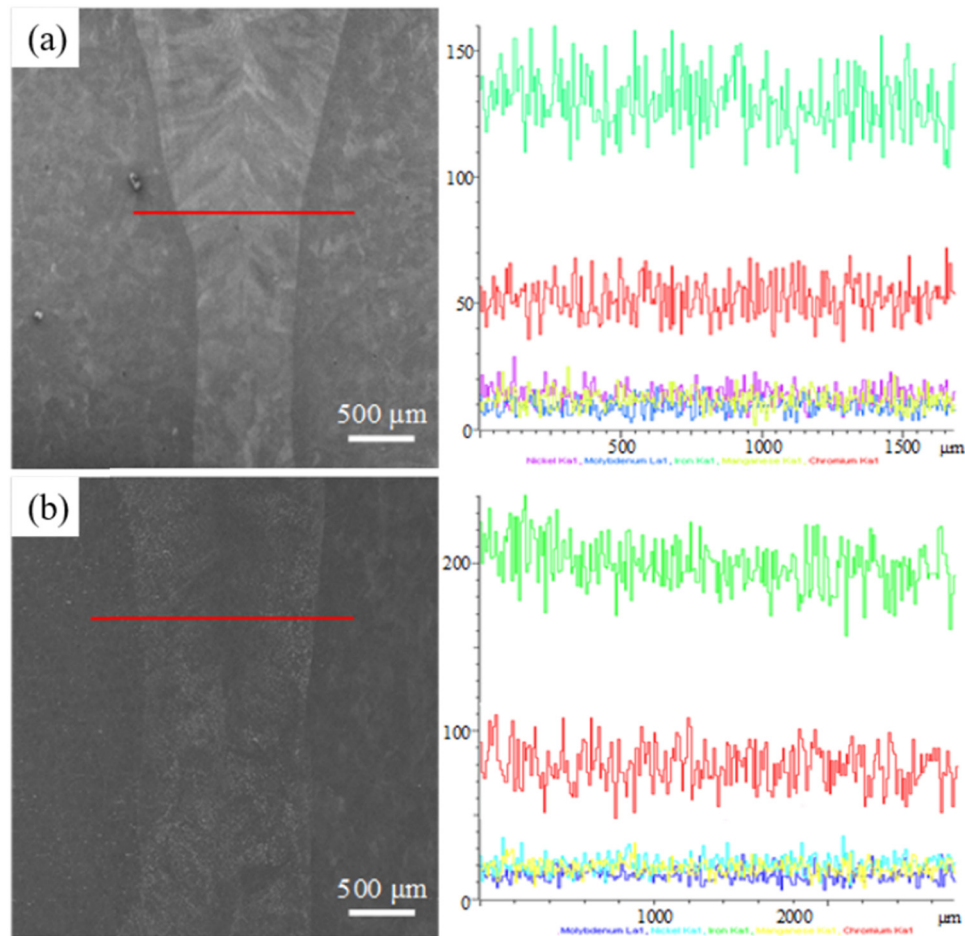


Figure 5: XRD diagrams of samples under different heat treatment conditions.



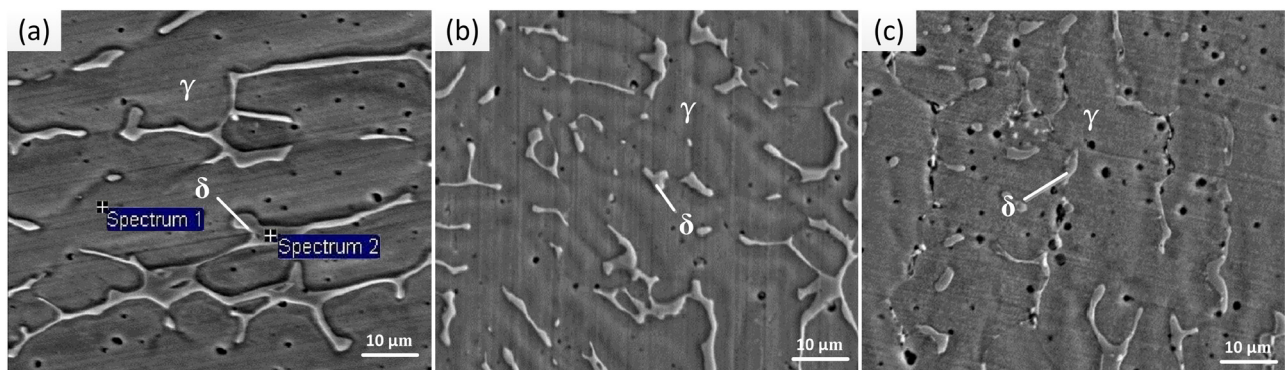


**Figure 6:** Line map of (a) AW joint and (b) ST joint.

low temperature heat treatment has no significant effect on the austenite columnar grains. The samples at 1,050°C for 30 min still mainly exhibit the austenite  $\gamma$  structure, but the diffraction peaks of (111)  $\gamma$ , (200)  $\gamma$  increased and the diffraction peaks of (220)  $\gamma$ , (311)  $\gamma$ , peaks decreased.

Moreover, a new diffraction peak (222) appears. It indicates that some austenite grains recrystallize and the orientation changes after heat treatment at 1,050°C.

The elemental line mapping across the joints of AW sample and ST sample were also performed, as shown in



**Figure 7:** SEM morphology of weld before and after heat treatment: (a) AW joint, (b) after annealing treatment at 400°C for 4 h, and (c) after ST at 1,050°C for 30 min.

**Table 4:** EDS analysis obtained from Figure 7 (wt%)

Spectrum	Phases	Cr	Ni	Fe	Mn	Mo	Si
1	$\gamma$	17.26	11.34	59.86	1.76	2.35	0.52
2	$\delta$	22.7	6.53	53.69	—	6.79	1.27

Figure 6, and there was no obvious variation noticed for Cr, Ni, Mo, and Fe at both sides of the weld.

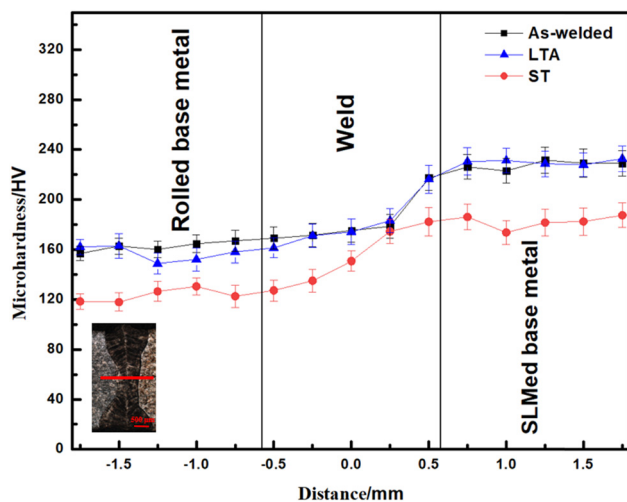
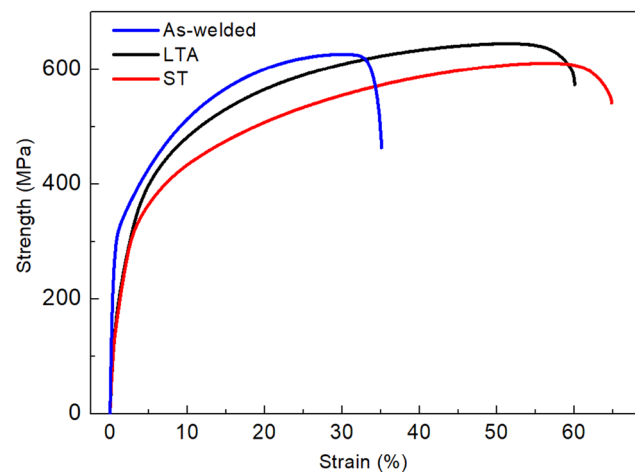
Figure 7 is the SEM morphology of weld before and after heat treatment. The microstructure of AW joint was composed of  $\gamma$  matrix and  $\delta$  phase distributed in dendritic pattern on the austenite matrix. The  $\delta$  phase was the crystal nucleus of the primary  $\delta$  ferrite left after the  $\delta \rightarrow \gamma$  transition. Due to short-range diffusion, the main element of ferrite Cr diffused from the austenite to the ferrite, in contrast, the dominant element of austenite Ni diffused and dispersed from the ferrite to the austenite [24], resulting in the Cr-poor and Ni-rich  $\gamma$  phase matrix and the Cr-rich and Ni-poor  $\delta$  ferrite in the crystal. The sampling points of energy dispersive spectroscopy (EDS) analysis of the weld are shown in Figure 7(a), and the analysis results are listed in Table 4.

The diffusion of carbon in  $\delta$  phase was more rapid than that in  $\gamma$  phase, but the solubility of carbon in ferrite was lower than that in austenite. During the cooling process, carbon in  $\delta$  phase was liable to be supersaturated, which promoted the precipitation and concentration of carbide  $M_{23}C_6$  inside the  $\delta$  phase. After the joint was annealing treated at 400°C for 4 h, the ferrite chains was “cut” or “break”, and its morphology changed from “dendrite” to “island,” as shown in Figure 7(b). After the joint was solution treated at 1,050°C for 30 min, the

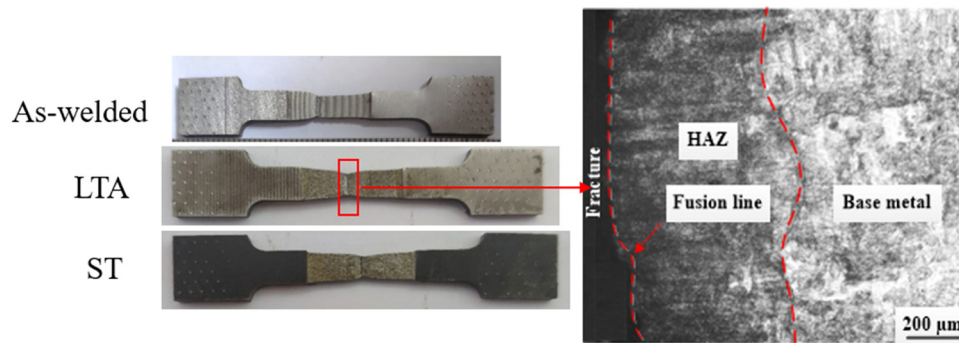
volume fraction of the  $\delta$  phase was further reduced, and the morphology acquired was wormlike. Usually, the  $\delta$  phase could hinder the movement of dislocations and grain boundaries, which might affect recrystallization and hinder the twin nucleation and growth processes [24]. Therefore, after heat treatment at 1,050°C, recrystallization occurred preferentially and unstrained crystal nuclei grew by the movement of the high-angle interfaces, forming coarse grains containing many twin boundaries, as shown in Figure 4(i).

### 3.2 Effect of heat treatment on mechanical property of welded joint

Figure 8 shows the microhardness variation across the dissimilar welds joint. The average hardness of the rolled-316 L base metal was measured  $168 \pm 5$  and  $232 \pm 4$  HV for SLMed-316 L steel. The hardness of weld decreased gradually from the SLM side to the rolled side. The hardness survey clearly showed the non-uniform hardness profiles along the welded joint. The higher hardness of SLM side is the layer-by-layer deposition characteristics of additive manufacturing which decided that it underwent rapid cooling and cyclic heating, which resulted in lattice distortion leading to the increase of microhardness. According to the previous microstructure analysis, the brittle hard phase  $M_{23}C_6$  precipitated from  $\delta$  phase and distributed inside  $\gamma$  phase, which increased the microhardness of the material to some extent [24]. The low temper annealing treatment alleviated the lattice distortion of the material and caused the precipitates to dissolve into the matrix and distribute

**Figure 8:** Microhardness distribution of laser-welded joints.**Figure 9:** Tensile test results of heat-treated samples.





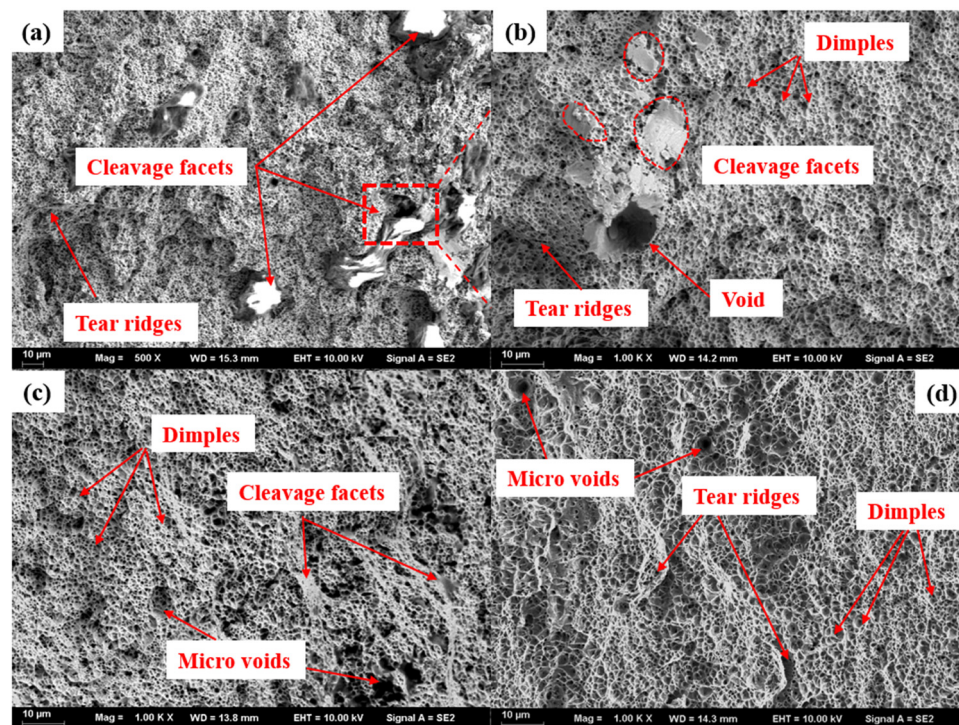
**Figure 10:** The photos of tensile test samples after tensile tests and OM image showing fracture path of laser-welded joint.

evenly, so that the microhardness of the material slightly decreased. After ST, a reduction in hardness of each zone of the welds joint was measured, which might be due to the evolution of the secondary phases at the inter-dendritic boundaries, the coarsening of the M<sub>23</sub>C<sub>6</sub> precipitates, and the dissolution of hard  $\delta$  phase into matrix [25].

Figure 9 shows the engineering stress–strain curves of the tensile samples of the as-built and heat-treated samples. The tensile strength measured of the AW joint was 630.4 MPa. After LTA, the tensile strength slightly changes, which was 643.6 MPa; after heat treatment at 1,050 C it decreased to 610.3 MPa. With the increase of heat treatment temperature, the yield strength gradually decreases. PWHT has little effect on tensile strength, but

played a significant role in improving ductility of welded joints. The ductility measured of AW joint was 35%, and increased to 60% in the LTA condition, both of which was less than that measured in the ST condition (65%).

The macroscopic fracture morphology of the different joints and OM image showing the fracture path of the laser-welded joint are displayed in Figure 10. All the tensile specimens were fractured in the weld with obvious necking in the break. The tensile fracture of the laser-welded joints occurred along with the fusion zone closer to the rolled parts rather than the base metals. This area was the columnar grain boundary, which was the most fragile part of the joint. The fracture of the joint between 316L stainless steel SLMed and rolled parts was characterized by typical ductile failure.



**Figure 11:** Fracture morphology of tensile specimen of: (a) AW joint, (b) enlarged detail of (a), (c) after LTA, and (d) after ST.

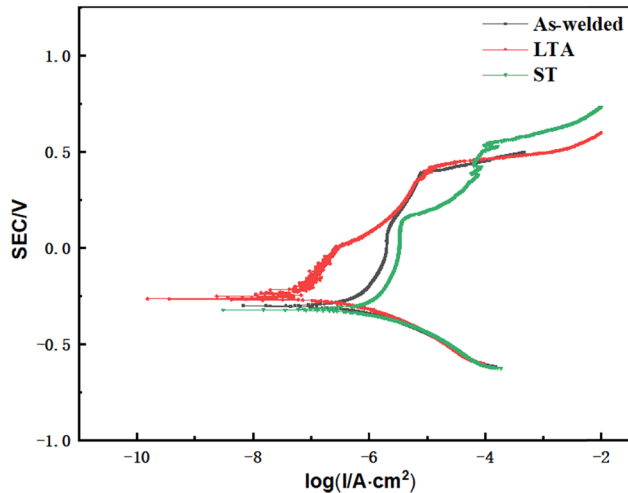


Figure 12: Planar polarization curve of the sample in hot place.

The fracture tensile specimen is shown in Figure 11. There were many dimples at the fracture morphologies of all samples, indicating that the fracture modes belong to plastic fractures in general. The fracture surface showed the tear ridges, cleavage facets, dimples, and microvoids with different sizes. In the AW joint, some cleavage facets, tear ridges, and voids along with fine size dimples were observed at the fracture surface, indicating that the fracture mode was mainly ductile fracture accompanied with some brittle fracture. The cracks may propagate along the ferrite. In the ST sample, cleavage facets and voids remained absent on the fracture surface but the size of the brittle area was decreased obviously as compared to the fracture surface in the AW joint. However, the amount of brittle area was less in the ST ones. In the ST sample, dimples of different sizes and depth were observed at the fracture surface, as shown in Figure 11(d).

According to Hall–Petch formula [26]:

$$\sigma_s = \sigma_i + kd^{-1/2} \quad (1)$$

where  $\sigma_s$  is the yield strength,  $\sigma_i$  is the dislocation movement resistance,  $k$  is the pinning constant, and  $d$  is the average grain size. It can be inferred that grain refinement resulted in improvement of tensile strength of the material. The change of the second phase (ferrite) would also affect

the yield strength. Previous articles had shown that less than 10% change of ferrite content had a less than 20 MPa effect on the yield strength [27,28]. In addition, heat treatment could also cause atomic diffusion to dissolve element segregation, such as the fusion lines. Chemical segregations would provide considerable strengthening (around 80 MPa) after heat treatment at 750–1,120°C, and the strengthening of element segregation would gradually decrease with the change of heat treatment temperature [29,30].

After LTA, the morphology of ferrite changed from the original skeleton or reticulated shape to granular or short rod-like shape and the fraction of the second phase decreased, so the yield and tensile strength decreased while the elongation increased slightly.

After heat treatment at 1,050°C, the ferrite was basically dissolved and the columnar austenite grains recrystallized, destroying the continuous grain boundaries along the building direction. The increase of grain size resulted in the decrease of dislocation density and grain coarsening; the tensile strength was significantly reduced after heat treatment at 1,050°C. There were discontinuous microcracks along the columnar grain boundaries. The microcracks consumed the slip activation energy and reduced the number of slip lines, which severely reduced the deformation degree and decreased the elongation of sample [31]. The microcracks decreased with the migration of grain boundaries, which increased the degree of deformation and improved the elongation sharply. Additionally, after heat treatment at 1,050°C, the grains recrystallized and the austenite columnar grains transformed into equiaxed annealing twin grains, which made the deformation more uniform and further greatly improved the elongation.

### 3.3 Effect of heat treatment on corrosion resistance of welded joint

Figure 12 shows the polarization curve of welded joints after heat treatment. The electrochemical parameters of partial corrosion of welded joints before and after heat treatment are detailed in Table 5. It is found that the

Table 5: Corrosion electrochemical parameters of welded joints

Sample	Corrosion potential (V)	Corrosion current density (A·cm <sup>-3</sup> )	Passive potential (V)	Passivity current density (A·cm <sup>-3</sup> )	Disruptive potential (V)
AW	-0.30	$1.2 \times 10^{-7}$	-0.045	$1.9 \times 10^{-6}$	0.37
LTA	-0.31	$1.28 \times 10^{-7}$	-0.042	$3.2 \times 10^{-6}$	0.18
ST	-0.257	$5.00 \times 10^{-8}$	—	—	0.41

pitting resistance of the welded joint after ST at 1,050°C for 30 min was the best, while the pitting resistance of the AW joint is the worst. Both the self-corrosion potential and the self-corrosion current density of welded joints have no obvious change after LTA, indicating that LTA has little effect on the corrosion tendency and corrosion resistance of welded joints. The phenomenon of slight change of the dimensional blunt current density, the significant decrease of the breakdown potential, and the significant shortening of the passivation interval indicated that the quality of the passivation film has increased, which made the long-term corrosion resistance of the joint improved.

Compared to the AW joints, heat treatment could effectively promote the dissolution of ferrite into austenitic matrix, and the fraction of  $\delta$  ferrite decreased with the rise of the heat-treated temperature. The corrosion resistance of the heat-treated joints enhanced owing to the dissolution of more  $\delta$  ferrite, the decreased Cr-depleted region, and the more compact passive film [32]. The secondary phases and element distribution play important roles in the corrosion resistance of laser-welded joints of SLM-316 L/rolled-316 L.

## 4 Conclusion

The weldability and the effect of post-heat treatment on the microstructure and mechanical properties of laser-welded joints of SLM-316 L/rolled-316 L were investigated in this study. The following conclusions have been drawn:

- (1) The obtained laser-welded joints of SLM-316 L/rolled-316 L were smooth and uniform without conspicuous defects such as cracks, pores, and non-fusions. The microstructure and the microhardness of joints showed obvious inhomogeneity. The joints had superior tensile strength but poor ductility compared with rolled-316 L metal.
- (2) The heat treatment temperature had a great influence on the microstructure evolution of laser-welded joints of SLM-316 L/rolled-316 L. Low temperature treatment had little influence on the microstructure, which desalinized granular or acicular ferrite morphology and eliminate the semi-melting zone. With the increase of temperature, the morphology of ferrite changed from the original skeleton or reticulated shape to granular shape. After ST, the ferrite was basically dissolved and the columnar austenite grains recrystallized, destroying the continuous grain boundaries and obvious grain coarsening was observed.
- (3) PWHT has little effect on tensile strength and corrosion resistance, but played a significant role in improving ductility of welded joints. The tensile strength of the AW joint was 630.4 MPa, which was 643.6 MPa after LTA, and 610.3 MPa after ST. The ductility of AW joint was 35%, and increased to 60% in the LTA condition, both of which was less than that measured in the ST condition (65%). After ST, the microhardness decreased slightly and the corrosion resistance had marginal improvement. A series of changes caused by PWHT, including the decrease of dislocation density, grain coarsening resulted by grain recrystallization, and the reduction of microcracks are the main factors for these performance variations of the joints.

**Acknowledgments:** The authors would also like to thank the support of the Analytical and Testing Center, JUST.

**Funding information:** This work was supported financially by the National Natural Science Foundation of China (NSFC, No. 51705218), Natural Science Foundation of China (NSFC, No. 51905231), and High-Tech Ship Scientific Research Project from the Ministry of Industry and Information Technology (No. [2019]360).

**Author contributions:** Hongwei Sun: conceptualization, investigation. Xiaopeng Lin: data curation, writing – original draft preparation. Xiaoyan Gu: resources, writing – review & editing, project administration, funding acquisition. Chenfu Fang: resources, validation, supervision. Zhidong Yang: resources, visualization.

**Conflict of interest:** Authors state no conflict of interest.

**Data availability statement:** The data that support the findings of this study are available from the corresponding author upon reasonable request.

## References

- [1] Nurhudan, A. I., S. Supriadi, Y. Whulanza, and A. S. Saragih. Additive manufacturing of metallic based on extrusion process: a review. *Journal of Manufacturing Processes*, Vol. 66, 2021, pp. 228–237.
- [2] Zhang, W. N., L. Z. Wang, Z. X. Feng, and Y. M. Chen. Research progress on selective laser melting (SLM) of magnesium alloys: a review. *Optik*, Vol. 207, 2020, id. 163842.
- [3] Rasoanarivo, F., D. Dumur, and P. Rodríguez-Ayerbe. Improving SLM additive manufacturing operation precision



- with H-infinity controller structure. *CIRP Journal of Manufacturing Science and Technology*, Vol. 33, 2021, pp. 82–90.
- [4] Yan, X., C. Chen, C. Chang, D. Dong, R. Zhao, R. Jenkins, et al. Study of the microstructure and mechanical performance of C-X stainless steel processed by selective laser melting (SLM). *Materials Science and Engineering: A*, Vol. 781, 2020, id. 139227.
  - [5] S. Periane, A. Duchosal, S. Vaudreuil, H. Chibane, A. Morandau, M. A. Xavier, et al. Influence of heat treatment on the fatigue resistance of Inconel 718 fabricated by selective laser melting (SLM). *Materials Today: Proceedings*, Vol. 46, 2021, pp. 7860–7865.
  - [6] Kale, A. B., P. Alluri, A. K. Singh, and S. H. Choi. The deformation and fracture behavior of 316 L SS fabricated by SLM under mini V-bending test. *International Journal of Mechanical Sciences*, Vol. 196, 2021, id. 106292.
  - [7] Kopf, R., J. Gottwald, A. Jacob, M. Brandt, and G. Lanza. Cost-oriented planning of equipment for selective laser melting (SLM) in production lines. *CIRP Annals*, Vol. 67, 2018, pp. 471–474.
  - [8] Sirohi, S., C. Pandey, and A. Goyal. Role of the Ni-based filler (IN625) and heat-treatment on the mechanical performance of the GTA welded dissimilar joint of P91 and SS304H steel. *Journal of Manufacturing Processes*, Vol. 65, 2021, pp. 174–189.
  - [9] Sirohi, S., A. Sauraw, A. Kumar, S. Kumar, T. Rajasekaran, P. Kumar, et al. Characterization of microstructure and mechanical properties of Cr-Mo Grade P22/P91 steel dissimilar welds for supercritical power plant application. *Journal of Materials Engineering and Performance*, Vol. 31, 2022, pp. 7353–7367.
  - [10] Karabulut, Y., E. Tascioglu, and Y. Kaynak. Heat treatment temperature-induced microstructure, microhardness and wear resistance of Inconel 718 produced by selective laser melting additive manufacturing. *Optik*, Vol. 227, 2021, id. 163907.
  - [11] Yan, X., S. Yin, C. Chen, C. Huang, R. Bolot, R. Lupoi, et al. Effect of heat treatment on the phase transformation and mechanical properties of Ti6Al4V fabricated by selective laser melting. *Journal of Alloys and Compounds*, Vol. 764, 2018, pp. 1056–1071.
  - [12] Liu, P., J. Y. Hu, H. X. Li, S. Y. Sun, and Y. B. Zhang. Effect of heat treatment on microstructure, hardness and corrosion resistance of 7075 Al alloys fabricated by SLM. *Journal of Manufacturing Processes*, Vol. 60, 2020, pp. 578–585.
  - [13] Åsberg, M., G. Fredriksson, and S. Hatami. Influence of post treatment on microstructure, porosity and mechanical properties of additive manufactured H13 tool steel. *Materials Science and Engineering: A*, Vol. 742, 2019, pp. 584–589.
  - [14] Shin, W. S., B. Son, W. Song, H. Sohn, H. Jang, Y. J. Kim, et al. Heat treatment effect on the microstructure, mechanical properties, and wear behaviors of stainless steel 316L prepared via selective laser melting. *Materials Science and Engineering: A*, Vol. 806, 2021, id. 140805.
  - [15] Maurya, A. K., C. Pandey, and R. Chhibber. Effect of filler metal composition on microstructural and mechanical characterization of dissimilar welded joint of nitronic steel and super duplex stainless steel. *Archives of Civil and Mechanical Engineering*, Vol. 22, 2022, id. 90.
  - [16] Ghorbani, S., R. Ghasemi, and R. E. Kahrizsangi. Effect of post weld heat treatment (PWHT) on the microstructure, mechanical properties, and corrosion resistance of dissimilar stainless steels. *Materials Science and Engineering: A*, Vol. 688, 2017, pp. 470–479.
  - [17] Jiang, Z., L. Ren, J. Huang, X. Ju, H. Wu, Q. Huang, et al. Microstructure and mechanical properties of the TIG welded joints of fusion CLAM steel. *Fusion Engineering and Design*, Vol. 85, 2010, pp. 1903–1908.
  - [18] Li, X., J. Chen, P. Hua, K. Chen, W. Kong, H. Chu, et al. Effect of post weld heat treatment on the microstructure and properties of Laser-TIG hybrid welded joints for CLAM steel. *Fusion Engineering and Design*, Vol. 128, 2018, pp. 175–181.
  - [19] Kumar, A. and C. Pandey. Autogenous laser-welded dissimilar joint of ferritic/martensitic P92 steel and Inconel 617 alloy: mechanism, microstructure, and mechanical properties. *Archives of Civil and Mechanical Engineering*, Vol. 22, 2022, id. 39.
  - [20] Dak, G. and C. Pandey. A critical review on dissimilar welds joint between martensitic and austenitic steel for power plant application. *Journal of Manufacturing Processes*, Vol. 58, 2020, pp. 377–406.
  - [21] Albright, C. E. and S. Chiang. High-speed laser welding discontinuities. *Journal of Laser Applications*, Vol. 1, 1988, pp. 18–24.
  - [22] Fabbro, R. Melt pool and keyhole behaviour analysis for deep penetration laserwelding. *Journal of Physics D: Applied Physics*, Vol. 43, 2010, id. 445501.
  - [23] Sirohi, S., C. Pandey, and A. Goyal. Characterization of structure–property relationship of martensitic P91 and high alloy ferritic austenitic F69 steel. *International Journal of Pressure Vessels and Piping*, Vol. 188, 2020, id. 104179.
  - [24] Moeini, G., S. V. Sajadifar, T. Wegener, C. Rössler, A. Gerber, S. Böhm, et al. On the influence of build orientation on properties of friction stir welded Al–Si10Mg parts produced by selective laser melting. *Journal of Materials Science & Technology*, Vol. 12, 2021, pp. 1446–1460.
  - [25] Pandey, C. Mechanical and metallurgical characterization of dissimilar P92/SS304 L welded joints under varying heat treatment regimes. *Metallurgical and Materials Transactions A*, Vol. 51, 2020, pp. 2126–2142.
  - [26] Wang, C., P. Zhu, Y. H. Lu, and T. Shoji. Effect of heat treatment temperature on microstructure and tensile properties of austenitic stainless 316L using wire and arc additive manufacturing. *Materials Science and Engineering: A*, Vol. 832, 2022, id. 142446.
  - [27] Pandey, C., N. Saini, M. M. Mahapatra, and P. Kumar. Study of the fracture surface morphology of impact and tensile tested cast and forged (C&F) Grade 91 steel at room temperature for different heat treatment regimes. *Engineering Failure Analysis*, Vol. 71, 2017, pp. 131–147.
  - [28] Hu, X., Z. Xue, G. Zhao, J. Yun, D. Shi, and X. Yang. Laser welding of a selective laser melted Ni-base superalloy: microstructure and high temperature mechanical property. *Materials Science and Engineering: A*, Vol. 745, 2019, pp. 335–345.
  - [29] Du, Z., H. C. Chen, M. J. Tan, G. Bi, and C. K. Chua. Investigation of porosity reduction, microstructure and mechanical properties for joining of selective laser melting fabricated aluminium composite via friction stir welding. *Journal of Manufacturing Processes*, Vol. 36, 2018, pp. 33–43.

- [30] Pandey, C., M. M. Mahapatra, P. Kumar, P. Kumar, N. Saini, J. G. Thakare, et al. Study on effect of double austenitization treatment on fracture morphology tensile tested nuclear grade P92 steel. *Engineering Failure Analysis*, Vol. 96, 2019, pp. 158–167.
- [31] Galy, C., E. Le Guen, E. Lacoste, and C. Arvieu. Main defects observed in aluminum alloy parts produced by SLM: From causes to consequences. *Additive Manufacturing*, Vol. 22, 2018, pp. 165–175.
- [32] Yang, J., Y. Wang, F. Li, W. Huang, G. Jing, Z. Wang, et al. Weldability, microstructure and mechanical properties of laser-welded selective laser melted 304 stainless steel joints. *Journal of Materials Science & Technology*, Vol. 35, 2019, pp. 1817–1824.